

Supporting Information

Adsorption capacity of the corrosion products of nanoscale zerovalent iron towards emerging contaminants

Junmin Deng^{1,2}, Sungjun Bae², Sunho Yoon², Mathieu Pasturel³, Rémi Marsac⁴, Khalil Hanna^{1,5*}

¹ Univ. Rennes, Ecole Nationale Supérieure de Chimie de Rennes, CNRS, ISCR-UMR 6226, F-35000, Rennes, France

² Department of Civil and Environmental Engineering, Konkuk University, 120 Neungdong-ro, Gwangjin-gu, Seoul 05029, Republic of Korea

³ Univ. Rennes, Université de Rennes 1, CNRS, ISCR – UMR6226, F-35000, Rennes, France

⁴ Univ. Rennes, CNRS, Géosciences Rennes - UMR 6118, F-35000 Rennes, France

⁵Institut Universitaire de France (IUF), MESRI, 1 rue Descartes, 75231 Paris, France

*Corresponding author: khalil.hanna@ensc-rennes.fr

14 pages: 11 Figures and 2 Tables

Supporting Information

Table S1. Mass balance in different reaction systems

Reaction systems	NA initial concentration (μM)	NA desorbed concentration (μM)
NZVI($0.2 \text{ g}\cdot\text{L}^{-1}$)		10.10
NZVI($0.2 \text{ g}\cdot\text{L}^{-1}$)+H ₂ O ₂ (0.5 mM)		10.04
NZVI($0.2 \text{ g}\cdot\text{L}^{-1}$)+H ₂ O ₂ (1 mM)	10	9.89
NZVI($0.2 \text{ g}\cdot\text{L}^{-1}$)+H ₂ O ₂ (2 mM)		9.88
NZVI($0.2 \text{ g}\cdot\text{L}^{-1}$)+H ₂ O ₂ (5 mM)		9.94
NZVI($0.2 \text{ g}\cdot\text{L}^{-1}$)+H ₂ O ₂ (10 mM)		9.92

Supporting Information

Table S2. Summary of the surface complexation model and parameters for the oxidized NZVI product.

Parameters	Value*
Site density (nm ⁻²)	1.50
Capacitance (F m ⁻²)	2.10
$\equiv\text{FeOH}_2^+ \rightleftharpoons \equiv\text{FeOH} + \text{H}^+$; pK _{a1}	5.19
$\equiv\text{FeOH} \rightleftharpoons \equiv\text{FeO}^- + \text{H}^+$; pK _{a2}	-7.82
log ^s K of oxidized NZVI	25.5

* W. Cheng, R. Marsac and K. Hanna, *Influence of Magnetite Stoichiometry on the Binding of Emerging Organic Contaminants, Environ. Sci. Technol., 2018, 52, 467-473.*

Supporting Information

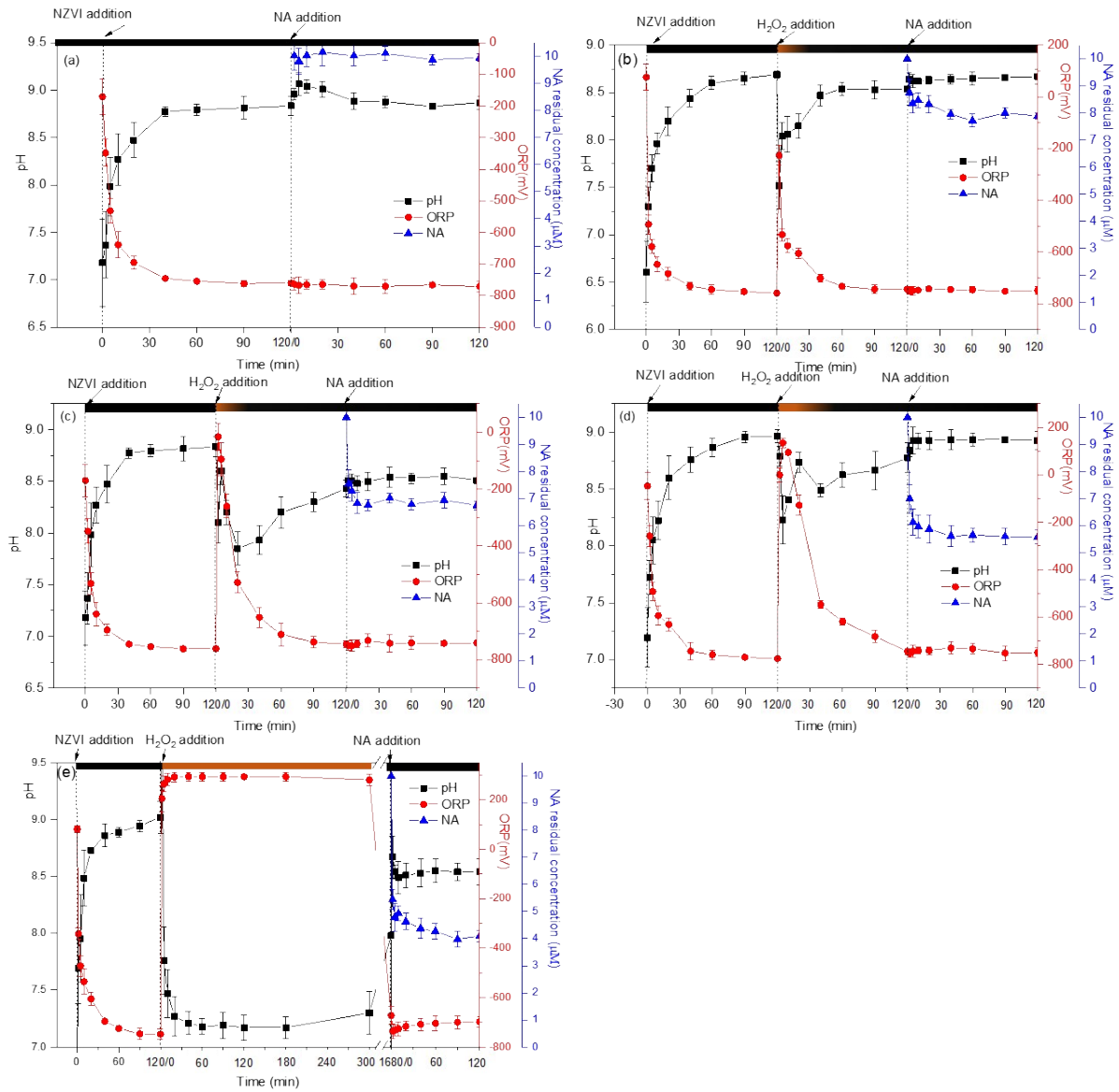


Figure S1. Variations in pH, ORP, color and NA concentration during NZVI oxidation and adsorption process at different H_2O_2 concentration (a) 0 mM; (b) 0.5 mM; (c) 1 mM; (d) 2 mM; (e) 10 mM. Experimental conditions: $[\text{NZVI}] = 0.2 \text{ g} \cdot \text{L}^{-1}$ $[\text{NA}]_{\text{initial}} = 10 \mu\text{M}$, $20 \pm 1^\circ\text{C}$.

Supporting Information

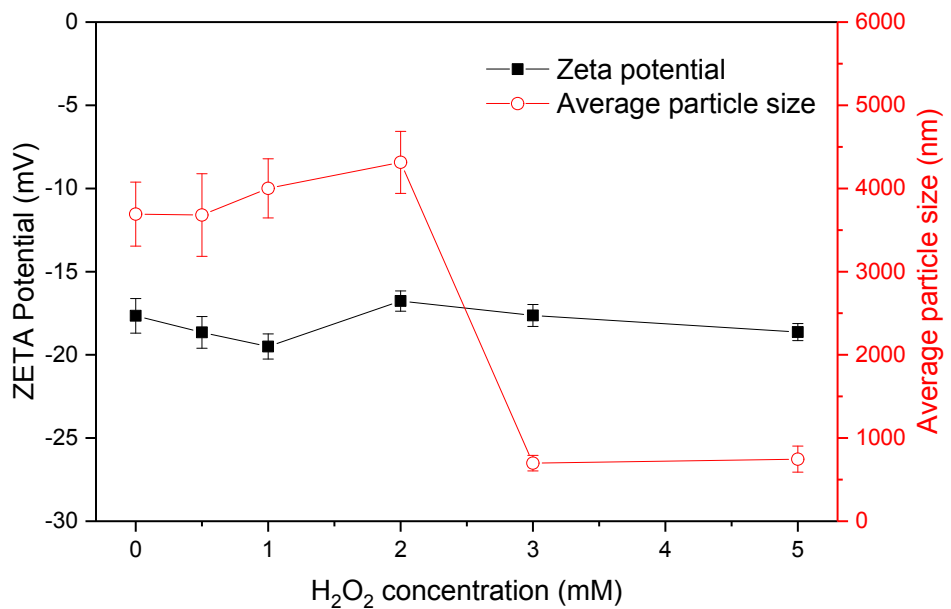


Figure S2. Zeta potential and average particle size of oxidized NZVI at different H_2O_2 concentrations. No dissolved Fe(II) concentration was detected under the experimental conditions of this study. Experimental conditions: $[\text{NZVI}] = 0.2 \text{ g}\cdot\text{L}^{-1}$, $[\text{H}_2\text{O}_2] = 5 \text{ mM}$, $I = 1 \text{ mM}$, $\text{pH } 9.0 \pm 0.2$, $20 \pm 1^\circ\text{C}$.

Supporting Information

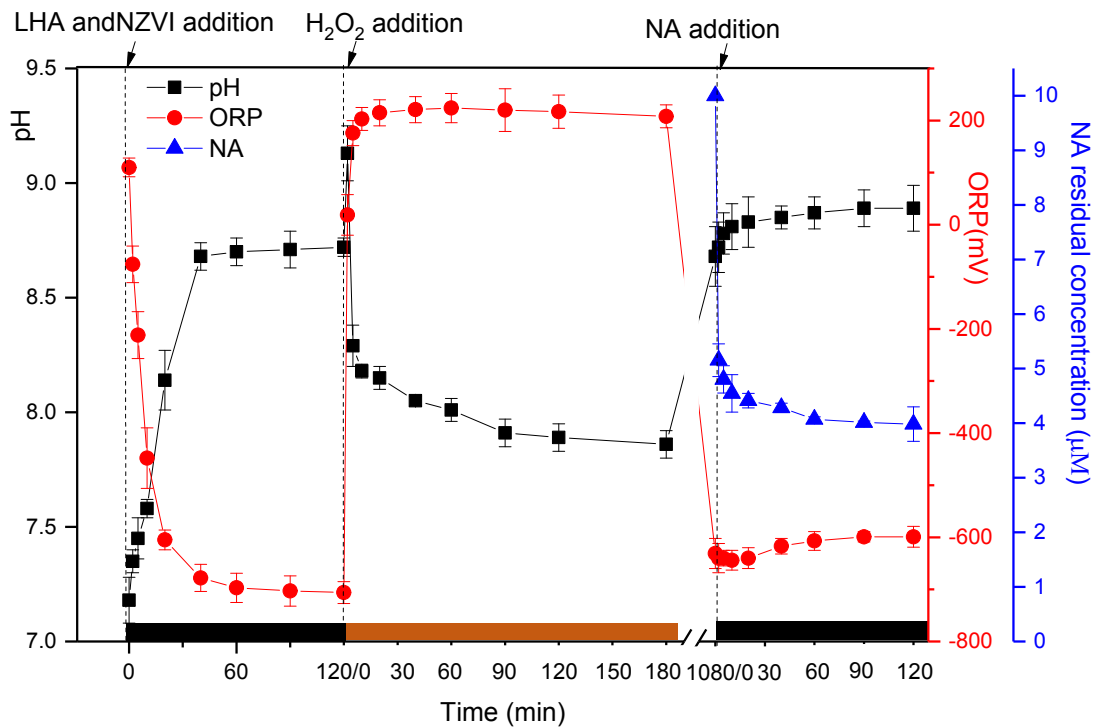


Figure S3. Variations in pH, ORP and NA concentration during NZVI oxidation and adsorption process at 2 mM H₂O₂ concentration with the presence of LHA. Experimental conditions: [LHA] = 5 mg·L⁻¹, [NZVI] = 0.2 g·L⁻¹, [H₂O₂] = 2 mM, [NA]_{initial} = 10 μM , 20 ± 1 °C.

Supporting Information

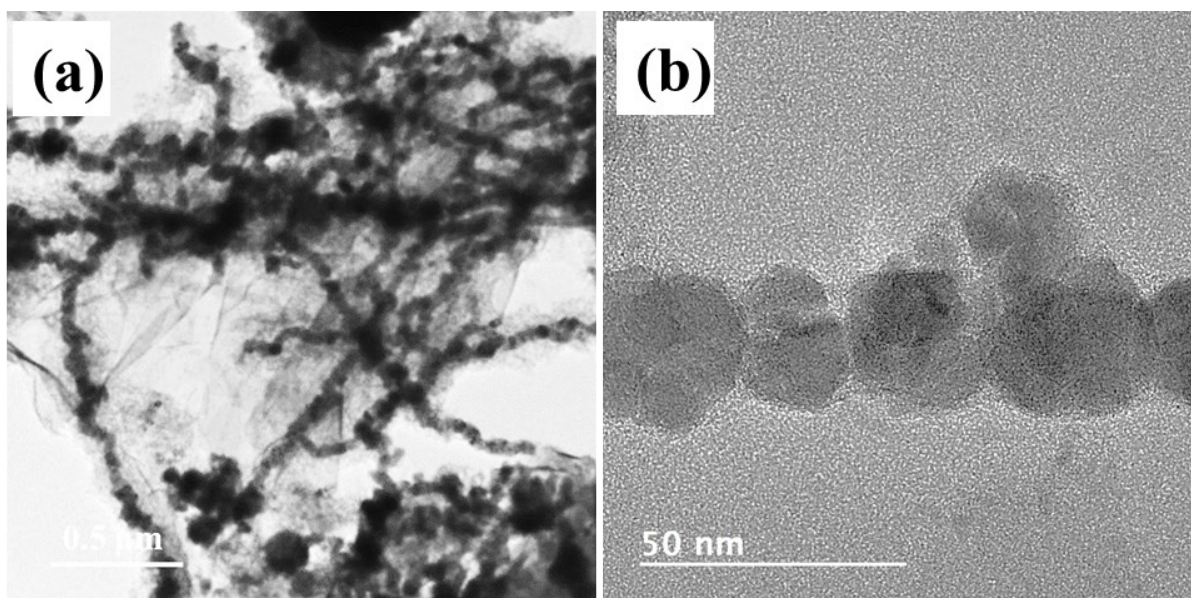


Figure S4. (a) Chain-like structures of oxidized NZVI; (b) constitution units of nano chain.

Experimental conditions: $[NZVI] = 0.2 \text{ g}\cdot\text{L}^{-1}$, $[\text{H}_2\text{O}_2] = 5 \text{ mM}$, 18h oxidation time, , $20 \pm 1 \text{ }^{\circ}\text{C}$.

Supporting Information

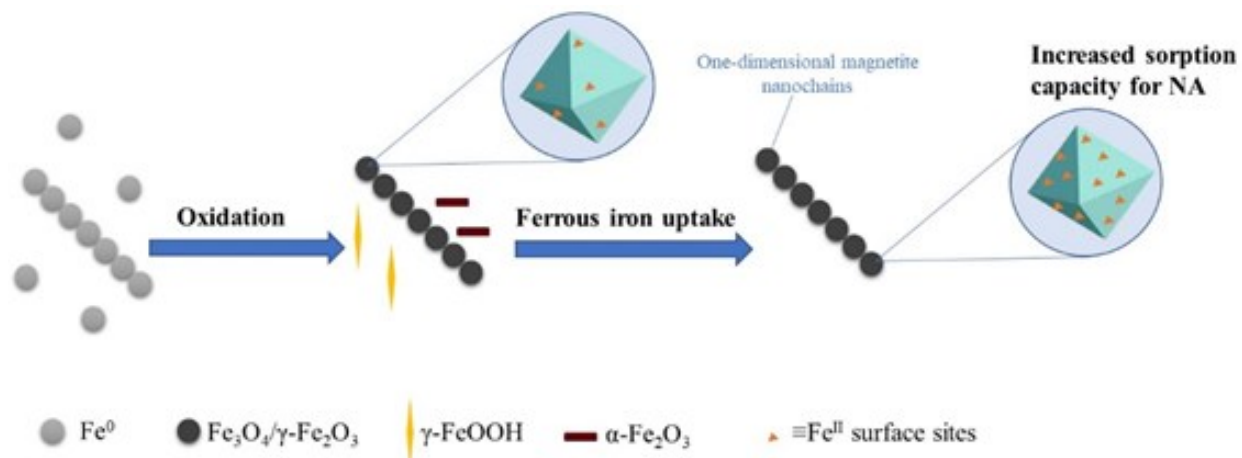


Figure S5. Schematic illustrating the oxidation process of NZVI by H_2O_2

Supporting Information

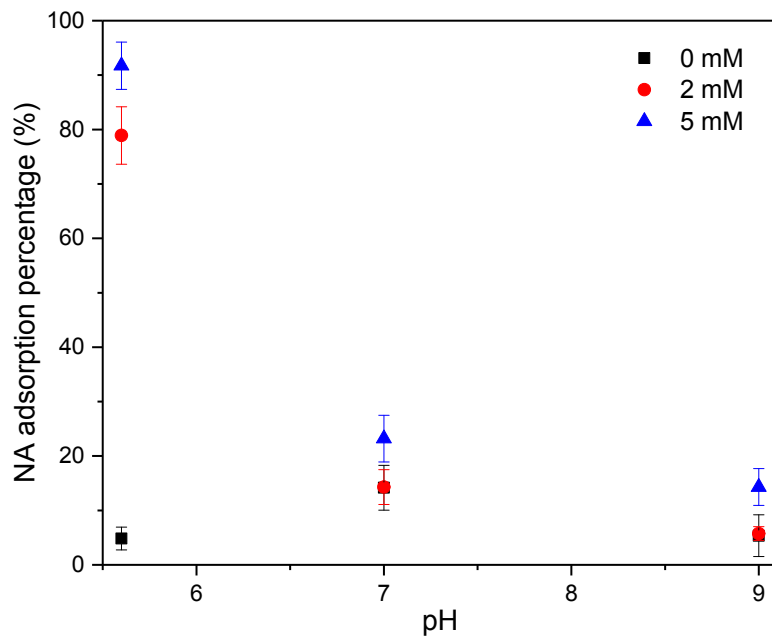


Figure S6. NA removal by the oxidized NZVI particles at two H_2O_2 concentrations in buffered systems. Experimental conditions: $[\text{NZVI}] = 0.2 \text{ g}\cdot\text{L}^{-1}$, $[\text{MES}] = 10 \text{ mM}$, $[\text{HEPES}] = 10 \text{ mM}$, $[\text{TRIZMA}] = 10 \text{ mM}$, $[\text{NA}]_{\text{initial}} = 10 \mu\text{M}$, $20 \pm 1^\circ\text{C}$.

Supporting Information

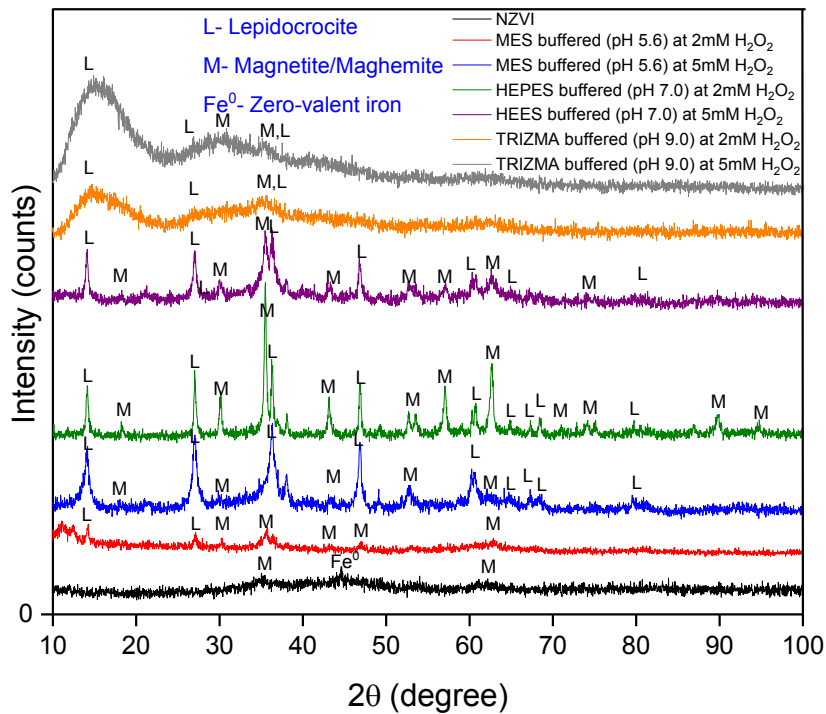


Figure S7. XRD patterns of NZVI oxidation products in buffered systems at two H_2O_2 concentrations. Experimental conditions: [NZVI]= 0.2 g·L⁻¹, [MES]=10 mM, [HEPES]=10 mM, [TRIZMA]=10 mM, [NA]_{initial}= 10 μM , $20 \pm 1^\circ\text{C}$.

Supporting Information

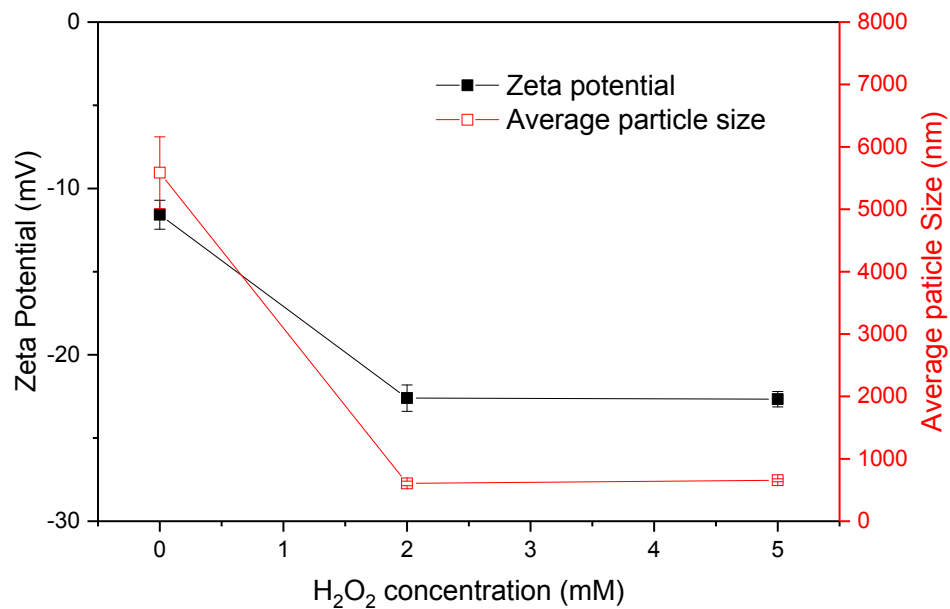


Figure S8. Zeta potential and average particle size of oxidized NZVI in TRIZMA buffered system (pH 9) at two H_2O_2 concentrations. Experimental conditions: $[\text{NZVI}] = 0.2 \text{ g/L}$, $[\text{TRIZMA}] = 10 \text{ mM}$.

Supporting Information

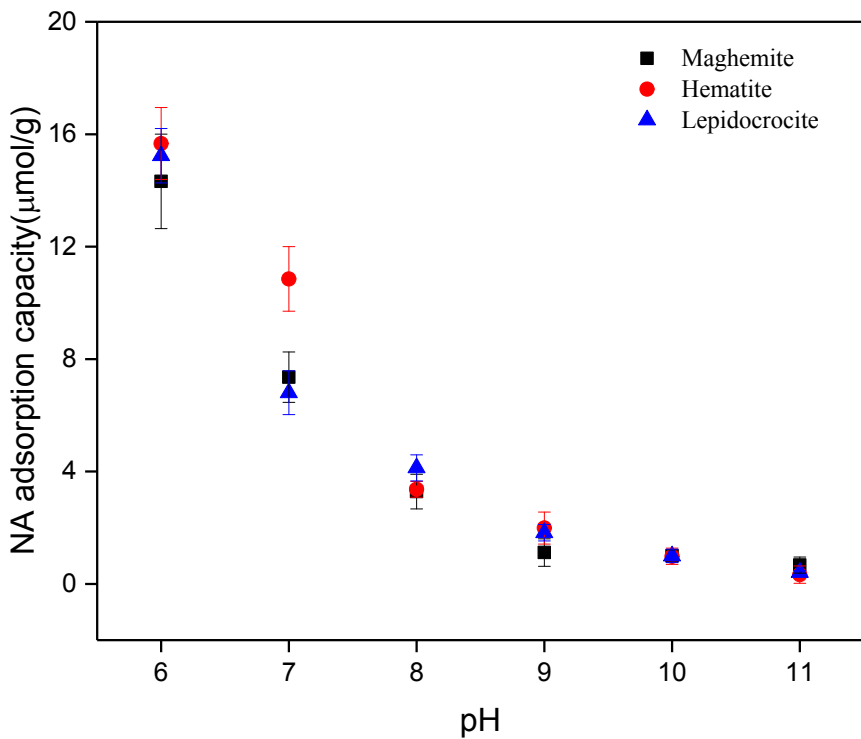


Figure S9. NA adsorption versus pH onto three ferric oxyhydroxides. Experimental conditions: [Maghemite] = 0.2 g·L⁻¹, [Hematite] = 0.2 g·L⁻¹, [Lepidocrocite] = 0.2 g·L⁻¹ [NA]_{initial} = 10 μM , 20 \pm 1 °C.

Supporting Information

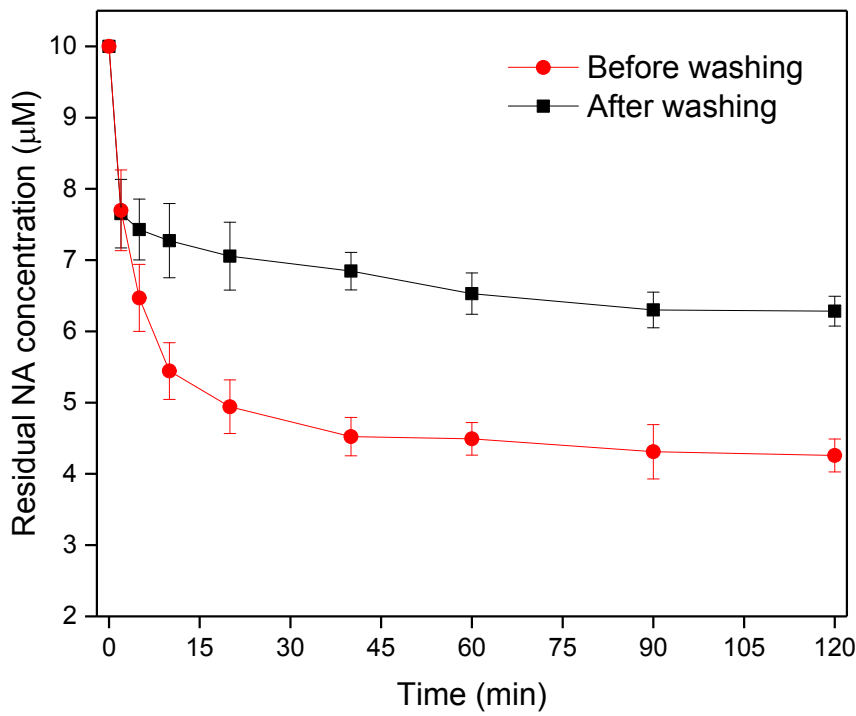


Figure S10. Adsorption kinetics of NA by oxidized NZVI at 5 mM of H_2O_2 before and after surface washing with DDIW. No dissolved Fe(II) concentration was detected under the experimental conditions of this study (*i.e.* pH 9). Experimental conditions: $[\text{NZVI}] = 0.2 \text{ g}\cdot\text{L}^{-1}$, $[\text{H}_2\text{O}_2] = 5 \mu\text{M}$, $[\text{NA}]_{\text{initial}} = 10 \mu\text{M}$, $\text{pH } 9.0 \pm 0.2$, $20 \pm 1^\circ\text{C}$.

Supporting Information

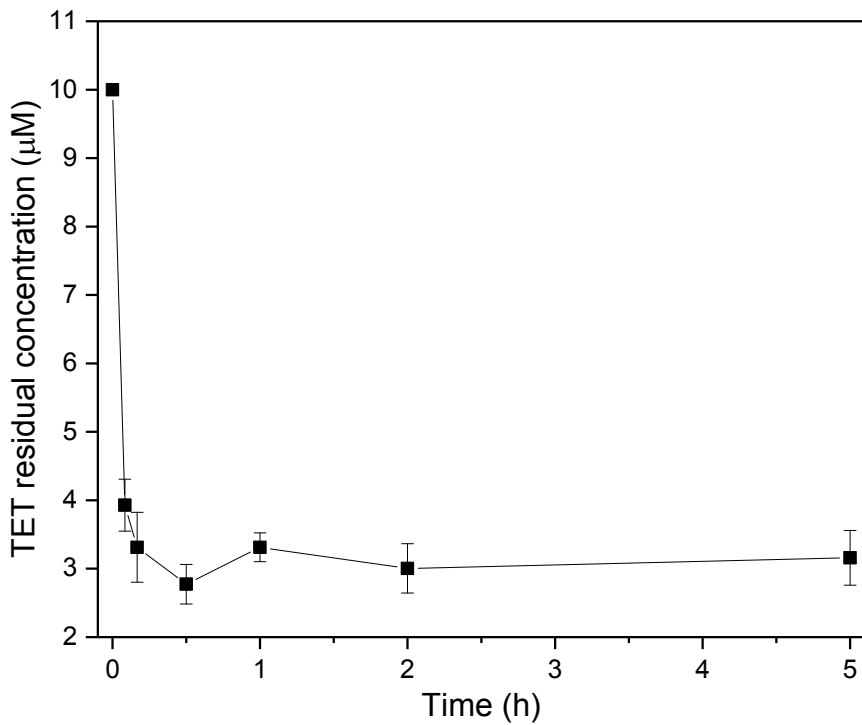


Figure S11. TET removal kinetics by the oxidized NZVI product at 5 mM H_2O_2 . Experimental conditions: $[\text{NZVI}] = 0.2 \text{ g}\cdot\text{L}^{-1}$, $[\text{H}_2\text{O}_2] = 5 \text{ mM}$, $[\text{TET}]_{\text{initial}} = 10 \mu\text{M}$, pH 9.0 ± 0.2 , $20 \pm 1^\circ\text{C}$.